Ocean Engineering 249 (2022) 110878

Contents lists available at ScienceDirect

Ocean Engineering

journal homepage: www.elsevier.com/locate/oceaneng

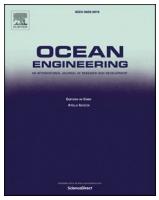

Hydrodynamic studies of floating structures: Comparison of wave-structure interaction modelling

W. Sheng [a], E. Tapoglou [b], X. Ma [a], C.J. Taylor [a], R.M. Dorrell [b], D.R. Parsons [b], G. Aggidis [a,*]

[a] Lancaster University Renewable Energy Group, Energy Engineering, Lancaster, United Kingdom
[b] University of Hull, Energy and Environment Institute, Hull, United Kingdom

ARTICLE INFO

Keywords:
WAMIT
NEMOH
HAMS
Wave-structure interaction
Free surface green function
Panel method

ABSTRACT

Current panel methods for wave-structure interactions employ the potential flow theory, which provide fast, reliable and relatively accurate predictions for the marine structures, and now some open source packages, NEMOH and HAMS, are available. In this research, the relative utility and performance of NEMOH and HAMS is compared with the well-known, state-of-art software, WAMIT. To bring focus to these comparisons, this research is based on three different floating structures: the truncated cylinder; the truncated cylinder with heave plate; and a novel multi-axis TALOS wave energy converter. To make the comparison more useful, this research investigates the incomplete and overlapped panels for the simple cylinder, to examine whether the respective code can handle these and still provide a meaningful solution. The comparisons may help us to understand whether the incomplete and/or overlapped panels can be used for simplifying the numerical modelling of those very complicated marine structures. From the comparisons, it can be seen the open source software, NEMOH and HAMS, both could produce very good results for the simple single marine structure, but also exhibit different capacities in dealing with more complicated marine structures. Specifically, HAMS could handle the thin structures and the overlapped panels effectively as WAMIT.

1. Introduction

Most of the existing panel methods for wave-structure interactions employ the potential flow theory including the commercial codes, such as, WAMIT (Ttd. https:/, 2021) and ANSYS AQWA (SA. https:, 2021). The similar type open source software are only available recently, including NEMOH (Babarit and Delhommeau, 2015) and HAMS (Liu, 2020, 2021), that have been released in 2014 and 2020, respectively, for public use free of charge. It should be noted that like many other codes and software packages, open source software would inherently have some limitations in their applications when compared to their commercial counterparts. This research makes some simulation-based quantitative comparisons between NEMOH and HAMS with the state-of-art commercial code, WAMIT, the most famous commercial panel code for wave-structure interactions, and frequently regarded as the industrial standard in the wave-structure interactions (Parisella and Gourlay, 2016; Kim et al., 1999).

To make these comparisons more focused and useful, this research examines three different floating structures, including: the simple truncated cylinder; the truncated cylinder with a heave plate and the TALOS point absorber wave energy converter. The simple truncated cylinder may be one of the most used and studied marine structures (Robertson et al., 2016; Greenhow and Ahn, 1988; Evans et al., 1979), due to axi-symmetry, which means the cylindrical marine structures would not be sensitive to the wave directions. The heave plates are the very useful marine structure components, which are widely used to enhance the hydrodynamic performance of the structure as required (Brown et al., 2017; Tao and Cai, 2004). The truncated cylinder with a heave plate is just one such marine structure, as shown in (Penalba et al., 2017). TALOS point absorber is the target marine structure for the TALOS multi-axis wave energy converter, which was proposed at Lancaster University (UK) and some initial investigations have been carried out, including the performance of the multi-axis PTO system (Aggidis and Taylor, 2017).

One of the aims of the research is to understand the potential for these two open source codes, so that it can become clearer in what situations the open source software is suitable and in what situations, the open source software has limitations, or even unsuitable. This research explains the limitations for HAMS and the reasons for the NEMOH failing in certain cases. Another purpose for this research is the

* Corresponding author.
E-mail address: g.aggidis@lancaster.ac.uk (G. Aggidis).

https://doi.org/10.1016/j.oceaneng.2022.110878
Received 4 November 2021; Received in revised form 15 February 2022; Accepted 18 February 2022
Available online 25 February 2022

expectation to identify a good hydrodynamic code (ideally an open source software), which can be used for optimising the TALOS point absorber wave energy converter as well as the multi-axis PTO system. Such a code should be accurate and reliable, even if some special components would be added to the point absorber, such as certain thin structures. In addition, the code must be fast, so that the optimisation of the wave energy converter would not be too expensive in relation to computational time.

All these three codes (WAMIT, NEMOH and HAMS) are based on the same principle: the flow is assumed as a potential (irrotational) flow, and solving the same boundary integral equations (Newman, 1977). To solve the boundary integral equation, all 3 codes require that the wet surfaces of the marine structures are discretised into small panels, and on the panels, the sources would be distributed. By solving the boundary integral equation, the strengths of the sources can be found (T and User Manual (v73)., 2021), and thus the solutions can be used for the modelling problems.

The key issue in establishing the simple boundary integral equation on the body surfaces is the employment of the free-surface Green function, which is a specific Green function that would satisfy the free-surface condition (with waves), the seabed condition and the wave radiation condition at infinity. However, such a free surface Green function itself would be a very complicated function, involving in an infinite integral, thus a complete calculation of the free surface Green function is generally prohibited. Instead, simple approximation methods must be found and implemented in the panel methods. The main difference among all these three codes is how the free surface Green function is approximated (Penalba et al., 2017; Newman, 1985; Liu et al., 2015):

- Based on the documents, WAMIT ('Wave Analysis MIT') implements the Newman's approximation methods for the calculation of free surface Green function, see details in (Newman, 1985; Newman et al., 1992). To the authors' knowledge, this 'core' method has been implemented in most commercial software packages of the panel method. Newman's approximation methods allow a fast and very accurate and reliable approximation to the free surface Green function, thus the integrals of the Green function and of its normal gradient on the panels. This may be the main reason why WAMIT is so successful that it provides the fast, reliable and accurate numerical simulations for many marine structures.
- HAMS ('Hydrodynamic Analysis of Marine Structures', by Dr. Yingyi Liu at Kyushu University, Japan (Liu, 2020; Liu, 2021)), is an open source code, in which the similar approximation methods have been implemented for the free surface Green functions (Liu et al., 2015; Wu et al., 2017, 2018). The software has been optimised for numerical modelling, thus it is fast (even faster than WAMIT for the examples used in the present research), accurate and reliable, but it has a large limitation: in current form, it can only be used for single marine structures, while multi-bodies are not an option yet.
- NEMOH is an open source code, released by Ecole Centrale de Nantes, France. Based on (Babarit and Delhommeau, 2015), the wave part of the Green function is calculated using an interpolation from a look-up table, so as to avoid the calculation or approximations of the Green function as seen in WAMIT and HAMS. In many applications, NEMOH could provide very good predictions to the problem, including multi-body interactions. However, we must note that it would not be as reliable in handling the cases when the target panel and the source panel are too close, such as the thin structures (Penalba et al., 2017) or the overlapped panels. Thus it may be limited for use in the marine structures with thin structures or the modelling with overlapped panels, as seen in an example in WAMIT (T and User Manual (v73)., 2021), where the overlapped panels are necessary for the internal tank modelling.

Open source software for modelling wave-structure interactions could provide options to meet challenges in ocean engineering, including simulation capacities, accuracy and running time. It is the purpose of this research to identify the capacities of the open source software, via the comparisons for different structures, as well as the relevant explanations why the open source software might fail in some specific problems. The overall target is to understand the open source software better, so to provide some guidance to choose which open source is best for different marine structures, if they are all suitable or only one of them is suitable.

The rest contents of the work are arranged as following: Section 2 briefly introduces the potential flow theory, with the concentrations on the free surface Green function, the relevant boundary integral equations and the frequency-domain dynamic equation for the structural motions; in Section 3, a brief introduction for the floating structures and the results of the hydrodynamic parameters and responses of three different panel codes are compared for three marine structures, including the added mass, the radiation damping coefficients, the wave excitations, and the motion responses; Section 4 makes the comparisons of the panel codes for the hydrodynamic parameters for the extreme cases of the incomplete and overlapped panels; while in Section 5, the software performance comparisons are made, including code capacity comparison and the speed comparison; and finally in the Section 6, the conclusions are given.

2. Brief introduction of potential flow theory

In this section, a brief introduction would be made for the potential flow theory for the panel method, with the concentrations on the approximations of free surface Green function, which could be an important factor in the panel methods, as in WAMIT, NEMOH and HAMS, and their capacities in dealing with the different marine structures.

2.1. Velocity potential functions

The potential flow theory involves the following assumptions:

- The flow is irrotational, thus the flow is a potential flow. The usefulness of an irrotational flow would be mainly dependent on the thickness of the boundary layer and how important the boundary layer would be for the problem.
- The flow is inviscid, but this assumption is basically redundant, because the assumption of the flow irrotationality also requires the flow to be inviscid.
- The fluid is incompressible. This assumption would be very practical, since the flow velocity in the wave-structure interaction is generally small.

The velocity potential function can be expressed as

$$\Phi\left(\vec{X},t\right)=Re\left[\varphi\left(\vec{X}\right)e^{i\omega t}\right] \tag{1}$$

where Φ is the actual velocity potential function, while φ is the complex amplitude of the velocity potential function, or more conventionally the frequency-domain potential function; $\vec{X}=(x,y,z)$ is the spatial vector, indicating the potential function and its complex amplitude are both space-dependent, and ω is the frequency of the dynamic system, with t being the time.

Both Φ and φ must satisfy Laplace's equation for the incompressible potential flow, as

$$\nabla^2\Phi=0;\ \nabla^2\varphi=0 \tag{2}$$

In a very fast calculation, as required for the wave-structure interactions, only the frequency-domain potential function, φ, is solved. For a given floating structure, the frequency domain potential function is only dependent on the frequencies of the incident wave. Of course, this is only possible if the governing equation and the relevant boundary

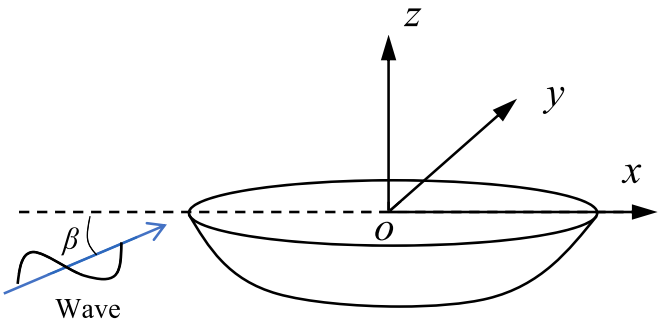

Fig. 1. The coordinate and the incident wave.

conditions are all linear.

To solve the Laplace equation for the frequency-domain potential function, φ, the boundary conditions for the wave-structure interaction must be applied, including:

- No-penetration boundary condition on the body surface

$$\frac{\partial \varphi}{\partial n} - \vec{V} \cdot \vec{n} = 0, \ on\ the\ body\ surface\ S_b \tag{3}$$

here $\vec{V}$ is the velocity vector of the body motion, $\vec{n}$ the unit vector normal to the body surface (pointing away from the fluid). This body surface boundary condition simply means the normal velocity of the structure is same as the normal velocity of the joint fluid.

- Seabed condition (no-penetration through the seabed)

$$\frac{\partial \varphi}{\partial z} = 0, \ at\ the\ seabed, \ z = -H \tag{4}$$

with H being the water depth.

- Linearised free surface boundary condition

$$\frac{\partial \varphi}{\partial z} - \frac{\omega^2}{g}\varphi = 0, \ at\ z = 0 \tag{5}$$

where g is the gravitational acceleration.

Thus it can be seen that the dynamic equation (Laplace equation) and the corresponding boundary conditions are all linear, therefore the superposition method can be employed to solve the potential function. And this is the reason why the time factor can be dropped as seen in the Eq. (1), and the frequency-domain potential function (hereafter simply the potential function) can be solved as expected.

2.2. Potential function decomposition

Based on the superposition principle, the potential function for the wave-structure interactions can be decomposed into the potential functions of wave radiation, φ_R and wave diffraction, φ_D. Following WAMIT (T and User Manual (v73)., 2021), the total potential function is given as

$$\varphi = \varphi_R + \varphi_D \tag{6}$$

1) Radiation problem

A radiation problem can be understood that the forced structure motion or the motion due to wave excitation would generate waves and the waves would radiate away from the structure. For the 6 degrees of freedom motion of a rigid body, the radiation potential functions include all the motion modes of the structure on the water surface, thus the radiation potential function can be expressed as a sum of 6 individual potentials, φ_j $(j = 1, 2, \ldots, 6)$, given as

$$\varphi_R = i\omega \sum_{j=1}^{6} \xi_j \varphi_j \tag{7}$$

This expression essentially follows the superposition principle, since the radiation potential functions would be all proportional to the motion amplitude, ξ_j. The individual radiation velocity potential, φ_j, can be understood as the potential function of a unit amplitude motion of the jth mode, while the factor '$i\omega$' in the expression of the radiation potential function is included so for simplifying the surface boundary condition, as

$$\frac{\partial \varphi_j}{\partial n} = n_j, \ on\ the\ body\ surface\ S_b \tag{8}$$

where n_j is the unit vector corresponding to the structural motion of jth motion mode. And based on the superposition principle, the individual potential function, φ_j, would satisfy the Laplace equation (2), the seabed condition (*4*) and free surface condition (*5*).

2) Diffraction problem

The diffraction problem can be understood as the case when the structure is stationary and due to the existence of the structure in water, the incoming wave would be diffracted by the structure. Hence the total potential function for the diffraction problem, φ_D, would be given as,

$$\varphi_D = \varphi_0 + \varphi_7 \tag{9}$$

here φ_0 is the velocity potential function of the incoming wave, which is given if the wave amplitude and frequency are known, and φ_7 is the potential function of the diffracted wave.

Based on the superposition principle, the diffraction velocity potential function φ_D would satisfy the Laplace equation (2), the seabed condition (*4*) and free surface condition (*5*), as

$$\frac{\partial \varphi_D}{\partial n} = 0, \ on\ the\ body\ surface\ S_b \tag{10}$$

or

$$\frac{\partial \varphi_7}{\partial n} = -\frac{\partial \varphi_0}{\partial n}, \ on\ the\ body\ surface\ S_b \tag{11}$$

3) Potential function of incoming wave

The velocity potential function of the incoming wave is specified by the wave amplitude, A, and the frequency, ω. In deep water, the velocity potential of the incoming wave is given as

$$\varphi_0 = \frac{igA}{\omega} e^{Kz} e^{-iKx\cos\beta - iKy\sin\beta} \tag{12}$$

where A is the wave amplitude, $K = \omega^2/g$ is the wave number in deep water, and β is the angle of incident wave, defined in Fig. 1.

In finite water depth, the velocity potential of the incoming wave is

$$\varphi_0 = \frac{igA}{\omega} \frac{\cosh k(z+H)}{\cosh\ kH} e^{-ikx\cos\beta - iky\sin\beta} \tag{13}$$

where H is the water depth, and the corresponding wave number in the finite water depth, k, can be solved or obtained using iteration method as the real root of the following dispersion relation:

$$\frac{\omega^2}{g} = k\ tanh\ (kH) \tag{14}$$

2.3. Boundary integral equation

Following the WAMIT manual (T and User Manual (v73)., 2021), for the radiation velocity potentials φ_j ($j = 1, \ldots, 6$), the boundary integral equation for solving the radiation potential function is given as

$$2\pi\varphi_j\left(\vec{X}\right) + \iint_{S_b} \varphi_j\left(\vec{X}_0\right) \frac{\partial G\left(\vec{X}_0; \vec{X}\right)}{\partial n} dS = \iint_{S_b} n_j\left(\vec{X}_0\right) G\left(\vec{X}_0; \vec{X}\right) dS \tag{15}$$

here $\vec{X} = (x, y, z)$ indicates the position vector of the field point, and $\vec{X}_0 = (x_0, y_0, z_0)$ the position vector of the source point, with $G(\vec{X}_0; \vec{X})$ being the free surface Green function.

And the boundary integral equation for solving the diffraction potential function, φ_7, is given as

$$2\pi\varphi_7\left(\vec{X}\right) + \iint_{S_b} \varphi_7\left(\vec{X}_0\right) \frac{\partial G\left(\vec{X}_0; \vec{X}\right)}{\partial n} dS = - \iint_{S_b} \frac{\partial \varphi_0\left(\vec{X}_0\right)}{\partial n} G\left(\vec{X}_0; \vec{X}\right) dS \tag{16}$$

In these boundary integral equations, the free-surface Green function, G, has been specially chosen to satisfy the free surface condition, the seabed condition, and the radiation condition at infinity automatically. By employing such a Green function, the integrals in the boundary integral equations (15) and (16) can be only on the body surfaces, S_b, while the integrals on the free surface, on the seabed, and at infinity (for radiation potentials) would all vanish. Such boundary integral equations for the radiation velocity potential functions, Eq.*(15)*, and for the diffraction potential function, Eq. (16), would have a huge advantage since in the integral equations, there is not a need to determine how large the free surface would be required in the numerical simulation.

The Green function that satisfies the free surface, the seabed conditions and the radiation condition at infinity, is given as follows. In deep water, the free surface Green function is given as

$$G\left(\vec{X}; \vec{X}_0\right) = \frac{1}{r} + \frac{1}{r'} + \frac{2K}{\pi} \int_0^\infty \frac{e^{\sigma(z+z_0)}}{\sigma - K} J_0(\sigma R)\, d\sigma \tag{17}$$

with

$$\begin{aligned} r &= \sqrt{(x-x_0)^2 + (y-y_0)^2 + (z-z_0)^2} \\ r' &= \sqrt{(x-x_0)^2 + (y-y_0)^2 + (z+z_0)^2} \\ R &= \sqrt{(x-x_0)^2 + (y-y_0)^2} \end{aligned} \tag{18}$$

and J_0 is the Bessel function of zero-order. The first two terms in the free surface Green function are the non-wave components, while the last term, the integral of limits from 0 to infinity is the wave part of the Green function.

In the finite water depth, the free-surface Green function is more complicated, defined as

$$G\left(\vec{X}_0; \vec{X}\right) = \frac{1}{r} + \frac{1}{r''} + 2 \times \int_0^\infty \frac{(\sigma + K)\cosh[\sigma(z+H)]\cosh[\sigma(z_0+H)]}{\sigma\, sinh(\sigma H) - K cosh(\sigma H)} e^{-\sigma H} J_0(\sigma R)\, d\sigma \tag{19}$$

here

$$r'' = \sqrt{(x-x_0)^2 + (y-y_0)^2 + (z+z_0+2H)^2} \tag{20}$$

Although the complicated form of the free surface Green function, the free surface Green function could significantly simplify the boundary integral equations, as seen in Eqs. (15) and (16): the surface integrals are only on the body surfaces.

In the panel method, the structure's wet surfaces would be discretised into many small panels (see Fig. 1). As such, the whole integral on the structure surface, S_b, would be made as the summation of the integrals on these small panels. Taking one surface integral in Eq. (15), the second term on the left-hand-side, it can be expressed as

$$\iint_{S_b} \varphi_j\left(\vec{X}_0\right) \frac{\partial G\left(\vec{X}_0; \vec{X}\right)}{\partial n} dS = \sum_{\ell=1(\ell\neq k)}^{N} \varphi_{j\ell} \iint_{\Delta S_\ell} \frac{\partial G_{\ell k}}{\partial n_\ell} dS \ (j = 1, \ldots 6) \tag{21}$$

It can be seen that on each small panel, the target potential φ can be taken as a constant, which is accepted since on the small panel, the variation of the target potential would not be large. However, the Green function must be carefully treated on the small panels, since it may change dramatically when the source and the field points are close, thus the calculation of the integral of the normal gradient of the Green function (and the integral of the Green function too) on the small panels is the key issue in the boundary integral method ((Newman, 1985; Liu et al., 2015; Newman et al., 1992; Wu et al., 2018; Wu et al., 2017)).

WAMIT and HAMS have implemented the very similar approximation methods for the free surface Green function (see (Newman, 1985; Newman et al., 1992) and (Liu et al., 2015)), while in NEMOH, the wave part of the free surface Green function is calculated using interpolation in a look-up table (Babarit and Delhommeau, 2015), for which the approximation of the Green function may be inaccurate when the source and field points are very close. Following table lists the approximation methods for the free surface Green function (the detailed approximation methods can be found in the corresponding references).

From the table, we can see both WAMIT (using the Newman's approximation (Newman et al., 1992)) and HAMS divide the entire fluid region into 4 sub-regions (however, they use different divisions for the fluid domain), while in NEMOH, the interpolation is used based on a pre-calculated look-up table of large entries, hence a large memory and a large computational time are required (Newman et al., 1992).

2.4. Hydrodynamic forces

Based on the solved boundary integral equation for the radiation potential functions, φ_j ($j = 1, 2, \ldots, 6$) and the diffraction potential function, φ_D, the corresponding hydrodynamic forces can be calculated. Following WAMIT (T and User Manual (v73)., 2021), for the radiation forces, they are given in terms of the added mass, $A_{jk}(j, k = 1, 2, \ldots, 6)$, and the damping coefficient, $B_{jk}(j, k = 1, 2, \ldots, 6)$, which can be calculated from the following equation,

$$A_{jk} - \frac{i}{\omega} B_{jk} = \rho \iint_{S_b} n_j \varphi_k dS \tag{22}$$

here we can see that the added mass is the real part of the integral of Eq. (22), and the radiation damping coefficient corresponds to the imaginary part of the above integral.

The wave exciting forces can be calculated directly from the diffraction potential function, φ_D, given as

$$F_j = -i\omega\rho \iint_{S_b} n_j \varphi_D dS \tag{23}$$

Or using the Haskind relation (T and User Manual (v73)., 2021), given as

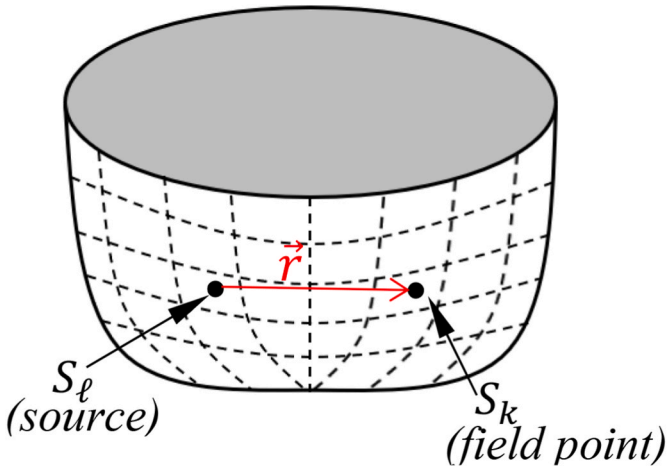

Fig. 2. The panels for the boundary integral equations.

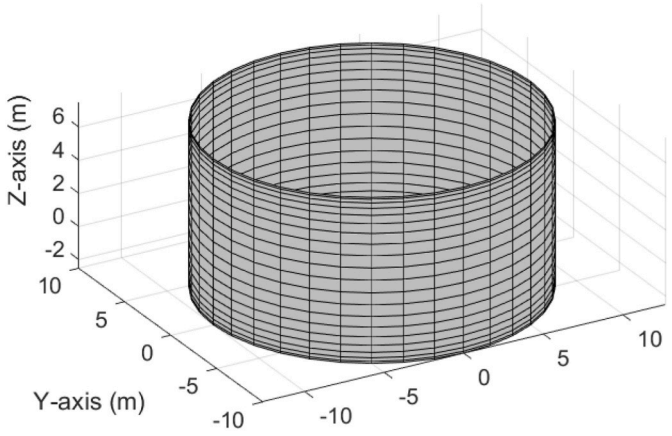

Fig. 3. The truncated cylinder (radius = 10 m, height = 10 m). Total panels: 1440. Panel file can be downloaded from (Sheng, 2022).

$$F_j = -i\omega\rho \iint_{S_b} \left(n_j \varphi_0 - \varphi_j \frac{\partial \varphi_0}{\partial n} \right) dS \tag{24}$$

2.5. Dynamic equation of the floating structure

The structural motion under the wave excitation would follow the Newton's 2nd law of motion, however, under the assumptions of the linear dynamic system, the structure motion can be carried out in the frequency domain in the panel methods.

Following WAMIT (T and User Manual (v73)., 2021), the frequency-domain dynamic equation of 6-degrees of freedom (DOFs) motions of a rigid structure is given in a form of mass-spring-damper system, as

$$\sum_{k=1}^{6} \left\{ -\omega^2 \left[M_{jk} + A_{jk}(\omega) \right] + i\omega B_{jk}(\omega) + C_{jk} \right\} \xi_k(\omega) = F_j(\omega) \tag{25}$$

where.

M_{jk}, C_{jk} are the matrices of the mass and the restoring coefficient matrix of the structure, respectively. The detailed calculations of these parameters can be found in the WAMIT manual (T and User Manual (v73)., 2021);

$A_{jk}(\omega)$, $B_{jk}(\omega)(j,\ k = 1, 2, \ldots, 6)$ are the matrices of the added mass and the radiation damping coefficient, and $F_j(\omega)(j = 1, 2, \ldots, 6)$ is the frequency-dependent complex amplitude of the wave excitation. All these can be calculated using the panel methods outlined above;

$\xi_k(\omega)(k = 1,\ 2, \ldots,\ 6,$ are the 6-DOF motions: surge, sway, heave, roll, pitch and yaw, respectively. This is the frequency-dependent complex amplitudes of motions, which is solved from the frequency-domain dynamic equation, Eq. (25). And in applications, the response amplitude operator (RAO) is the more useful expression, defined as

$$\chi_k = \frac{\xi_k}{A} \tag{26}$$

Obviously for the wave of a unit amplitude, the frequency-dependent ξ_k itself is the RAO.

In the conventional plots, the module of the RAO is used to see the actual response of the structural motion in waves, calculated as

$$|\chi_k| = \frac{|\xi_k|}{A} \tag{27}$$

3. Floating structures and their hydrodynamic analyses

In this section, the introduction of three floating structures is given first, and then the hydrodynamic parameters and responses are compared, including: added mass, radiation damping coefficients, the wave excitations and the response amplitude operators (RAOs). All the comparisons are made for 3 motion modes: surge, heave and pitch.

3.1. Introduction of the floating structures

To bring focus to this comparison, some simple but yet important marine structures are studied in this investigation, and these three different structures are: the truncated cylinder; the truncated cylinder with a heave plate and the TALOS point absorber.

3.1.1. Truncated cylinder

The truncated cylinders may be the most popular marine structures due to their axi-symmetry, which means they would be insensitive to the directions of incoming waves. Also if the length of the truncated cylinder is extended, it would become a spar, another popular marine structure (Falcao et al., 2012; Wang et al., 2008; Tao et al., 2000). Hence it is important to see how the open source software in handling this simple structure.

Here a truncated cylinder of radius 10 m and height 10 m is considered (Fig. 2). The centre of gravity of the marine structure in this comparison is taken as z = −7.5 m (it is lower than the centre of buoyancy), so to guarantee the stability of the cylinder (with a positive initial metacentric height).

3.1.2. Truncated cylinder with a damping plate

The difference of this structure with the simple truncated cylinder is the heave plate, see Fig. 3. As in the practical applications, heave plates are generally used to enhance the performance of the structure motions in waves. Due to the thin structure nature, the boundary element method (BEM) analyses would be challenging in generating the good panels for simulation: the very fine panels must be generated at the side of the thin structure, and accordingly, the panels near the side must be fine enough so to satisfy the general rule of the panel generation for panel methods. As a result, the total number of panels for the structures with thin components would be very large in numerical modelling. In addition, such thin structures may also make the target panel and source panel becoming too close, thus to cause the problems of the numerical modelling. The structure with a heave plate is used to check how the open source software can handle the thin structure effectively in the numerical modelling.

3.1.3. TALOS wave energy converter

TALOS is an enclosed multi-axis point absorber wave energy converter, which was proposed by Prof. George Aggidis (Aggidis and Taylor,

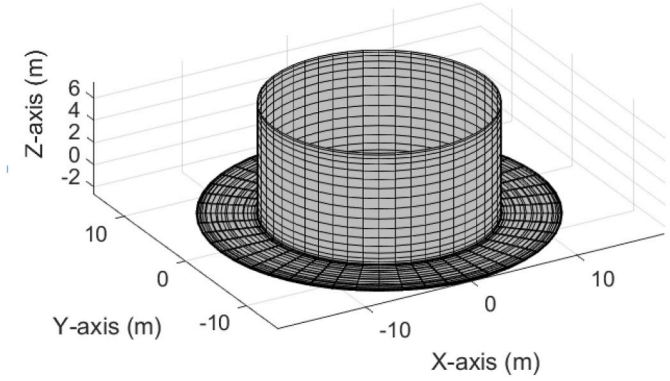

Fig. 4. The truncated cylinder (radius = 10 m, height = 10 m), with a damping plate (radius = 15 m, thickness = 0.1 m). Total panels: 3072. Panel file can be downloaded from (Sheng, 2022).

2017; Zhang et al., 2015). The wave energy converter incorporates the use of a heavy ball so for the multi-axis energy conversion. At Lancaster University (UK), some initial investigations have been carried out, see the design of TALOS I (Fig. 4a) and TALOS II (Fig. 4b). And in the drawing of TALOS II, we can see the heavy ball and the PTO system clearly from the cut-off (Fig. 3b). A damper test rig is also designed for testing the multi-axis power take-off system, see Fig. 4c.

The TALOS wave energy converter would have some advantages when compare to other types of wave energy converters including:

- TALOS is a multi-axis PTO system for converting wave energy into electricity, which could absorb energy from all motion modes of the structure motions;
- TALOS is a fully enclosed wave energy converter, thus PTO is less subjected to severe marine environments;

In this research, the TALOS hull is based on the concept TALOS I, which has an octagonal section. The TALOS in this research has a maximum width of 30 m, an overall draft of 17.6 m (the lower octagonal cylinder has a length 13.1 m). Fig. 5 shows the panels for the wet surfaces for hydrodynamic analysis, and the arrangement of the PTOs in the TALOS I would be very similar as seen in the TALOS II. However, this research concentrates in the overall hydrodynamics of the hull, thus PTOs will not be applied in this research. The overall sizes of the TALOS I structure can be seen in Fig. 5, and the panels for the wet surfaces of the marine structure.

3.2. Results of hydrodynamic analyses

This section focuses on the analyses and comparisons of the hydrodynamic forces, including the parameters related to the wave radiation in terms of added mass and radiation damping coefficient, and the wave excitation acting on the structure.

3.2.1. Truncated cylinder

For this simple marine structure, the predictions of the hydrodynamic parameters are all very close. Fig. 6 shows the hydrodynamic parameters for the surge motion of the truncated cylinder: the added mass, A_{11}, the radiation damping coefficient, B_{11}, and the wave excitation force, F_{ex1} (against the wave period, T). They are all very close to the predictions of WAMIT. For HAMS, the predictions are almost identical to those of WAMIT, except at the irregular frequency (period), while NEMOH slightly overpredicts the added mass, radiation damping and the wave excitation.

The sharp variations at the irregular frequency are the nature for such panel methods, and the remedy can be either by reducing the size of panels, but it would move the irregular frequency to a higher frequency; or using the option of the removal of irregular frequency as available in both WAMIT (T and User Manual (v73)., 2021) and HAMS (Liu, 2020) (no such option available in the current NEMOH). However, the irregular frequency is a high frequency regarding to the floating structures and waves, hence in most practical problems, such sharp variations at the irregular frequency are not the concern for the study on wave-structure interaction, and this is especially true for wave energy converters, since in the waves of high frequencies, the wave energy density is small.

Fig. 7 shows the hydrodynamic parameters for the heave motion of

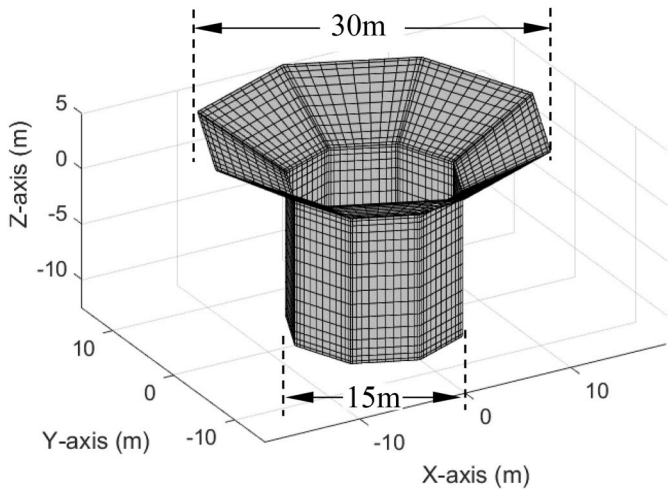

Fig. 6. TALOS is a point-absorber structure, which was designed to implement the multi-axis power take-off (PTO). The overall structure is octagonal following the original design, but the size of the structure has been halved, with the maximal width = 30 m at the top (calm water plane), and the maximal width = 15 m for the octagonal prism below. Total panels:1632 (with a symmetry about y-axis).

Fig. 5. TALOS I and TALOS II (with the proposed PTO system), and the PTO test rig (Aggidis and Taylor, 2017).

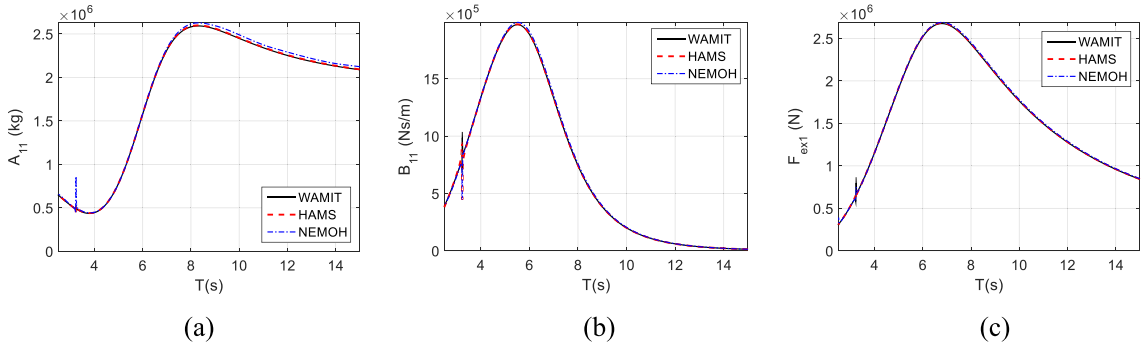

Fig. 7. Added mass (a), radiation damping coefficient (b) and wave excitation force (c) for surge motion (truncated cylinder).

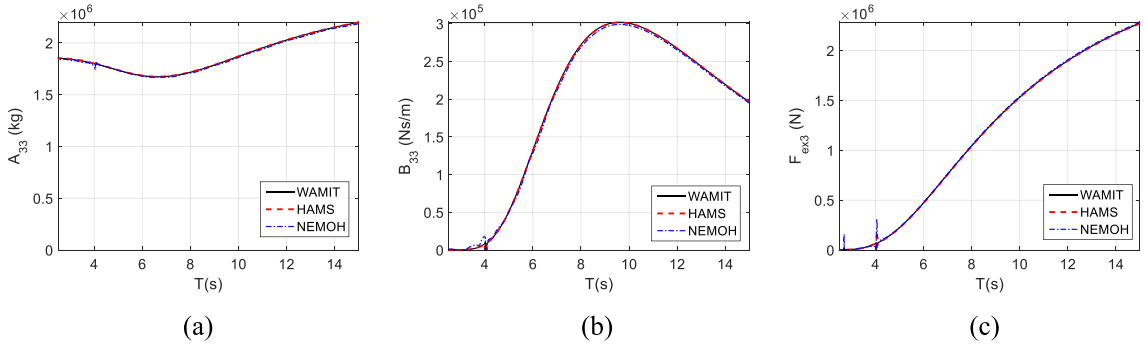

Fig. 8. Added mass (a), radiation damping coefficient (b) and wave excitation force (c) for heave motion (truncated cylinder).

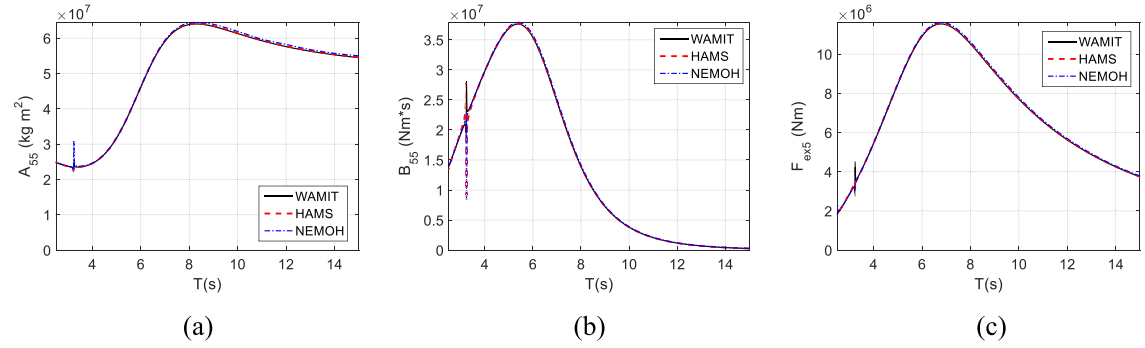

Fig. 9. Added mass (a), radiation damping coefficient (b) and wave excitation force (c) for pitch motion (truncated cylinder).

the truncated cylinder: the added mass, A_{33}, the radiation damping coefficient, B_{33}, and the wave excitation force, F_{ex3}. Again, they are all very close to the predictions of WAMIT, and for HAMS, they are almost identical to those of WAMIT. NEMOH slightly under-predicts the added mass, and the radiation damping for heave motion, while the wave excitation is almost identical as that of WAMIT.

Fig. 8 shows the hydrodynamic parameters for the pitch motion of the truncated cylinder: the added moment of inertia, A_{55}, the radiation damping coefficient, B_{55}, and the wave excitation moment, F_{ex5}. It can be seen that both NEMOH and HAMS predictions are almost identical to those of WAMIT, except those at the irregular frequency (period).

From all these comparisons, it can be seen that all the predictions from the different software are acceptable for engineering applications for this simple marine structure.

3.2.2. *Truncated cylinder with a heave plate*

A heave plate is a large thin horizontal plate (other possible orientations of the thin plate are possible, then they should be called different names). Since a heave plate is very thin (0.1 m thick), the heave plate itself would add a small displacement to the displacement of the truncated cylinder. When in waves, a heave plate could significantly increase the added mass, and change the damping coefficient and wave excitation, thus a significant change of the hydrodynamic performance can be possible.

Fig. 9 shows the hydrodynamic parameters for the surge motion of the truncated cylinder with a heave plate: the added mass, A_{11}, the radiation damping coefficient, B_{11}, and the wave excitation force, F_{ex1}. In the comparison, the thin plate is also represented using dipoles (the option only by WAMIT), in which the heave plate is taken as a structure of zero thickness, and both sides of the structure are wet (the conventional surface is wet only on one side). Such a simplification allows relative coarse panels on the heave plate, and thus there would be no difficulties in numerical modelling, thus it is generally regarded the best option for the thin structure.

It can be seen all predictions are very close to the predictions of WAMIT (with the thin structure) and of WAMIT with dipoles. No significant difference can be discerned for all predictions, except at the irregular frequency (period) at which frequency, the panel method

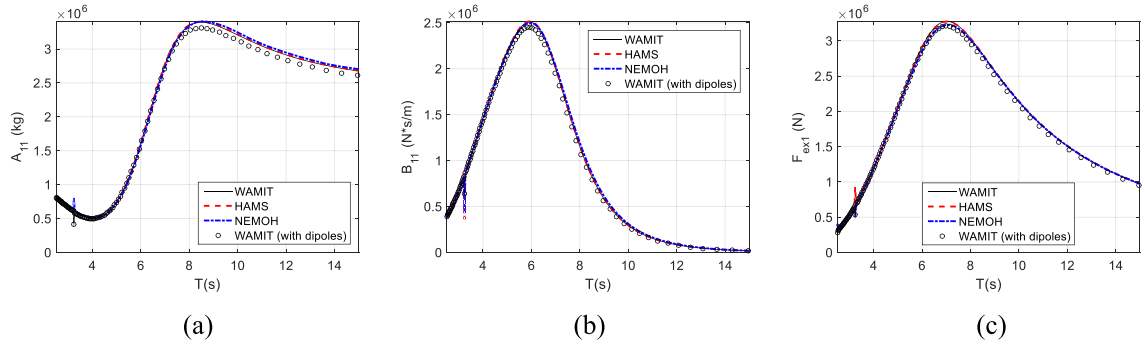

Fig. 10. Added mass (a), radiation damping coefficient (b) and wave excitation force (c) for surge motion (truncated cylinder with heave plate).

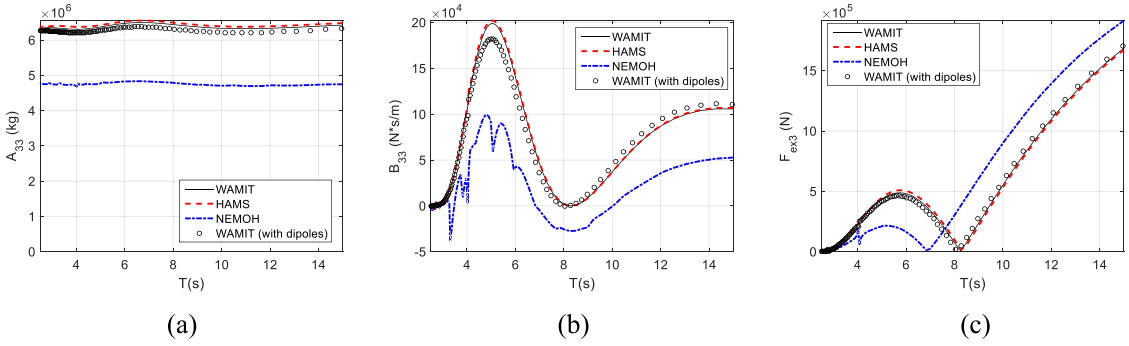

Fig. 11. Added mass (a), radiation damping coefficient (b) and wave excitation force (c) for heave motion (truncated cylinder with heave plate).

Table 1
The subregion definitions for approximating the free surface Green function.

Sub-region	WAMIT (Newman et al., 1992)	HAMS (Liu et al., 2015)	NEMOH
1	$0 \le X \le 3; 0 \le Y \le 4$	$\frac{R}{H} \ge 0.5$	Interpolation using the pre-calculated look-up table. Based on (Newman et al., 1992), Large tables are required in building the look-up table, including 64,000 to 2,000,000 entries.
2	$3 \le X \le \infty; 0 \le Y \le 4$	$0.05 \le \frac{R}{H} < 0.5$	
3	$0 \le X \le 3; 4 \le Y \le \infty$	$0.0005 \le \frac{R}{H} < 0.05$	
4	$3 \le X \le \infty; 4 \le Y \le \infty$	$\frac{R}{H} < 0.0005$	
Definitions of parameters	$X = KR$; $Y = K\lvert z+H\rvert$ [17] K: wave number in deep water $R = \sqrt{(x-x_0)^2 + (y-y_0)^2}$ (x, y): for the field point; (x_0, y_0) : for the source point H: water depth		No more details available

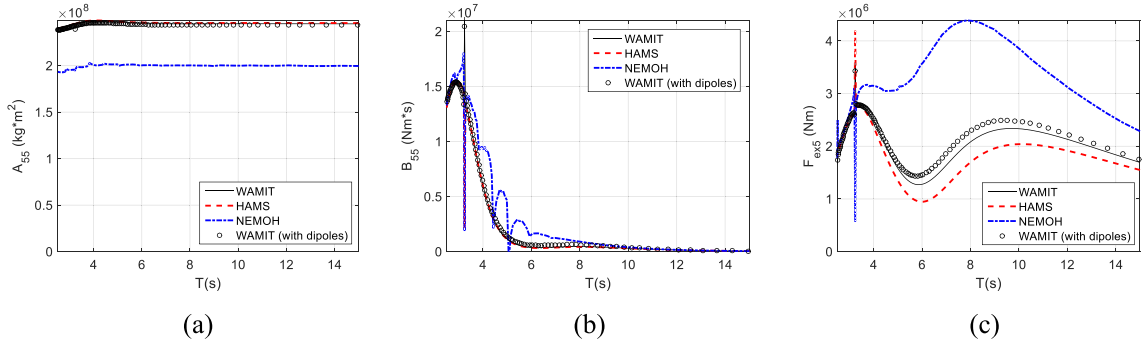

Fig. 12. Added mass (a), radiation damping coefficient (b) and wave excitation force (c) for pitch motion (truncated cylinder with heave plate).

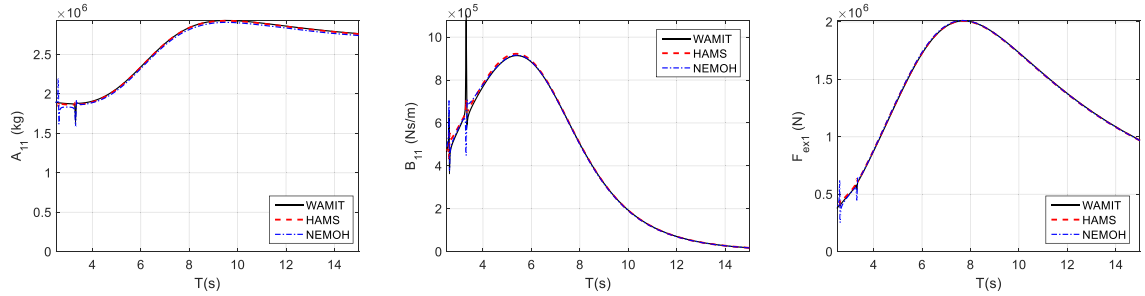

Fig. 13. Added mass (a), radiation damping coefficient (b) and wave excitation force (c) for surge motion (TALOS device).

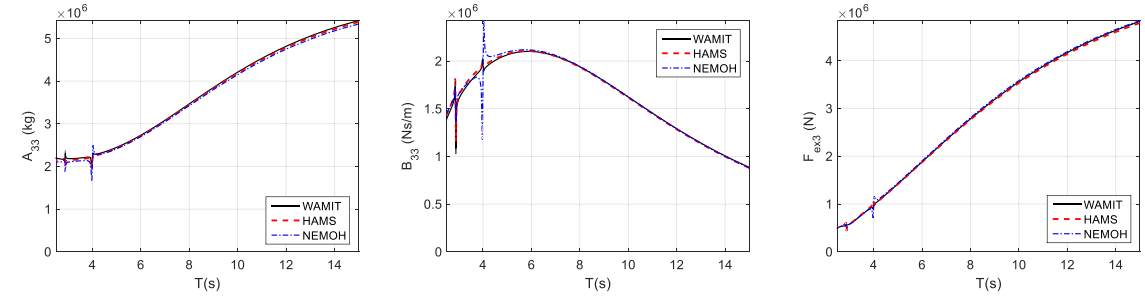

Fig. 14. Added mass (a), radiation damping coefficient (b) and wave excitation force (c) for heave motion (TALOS device).

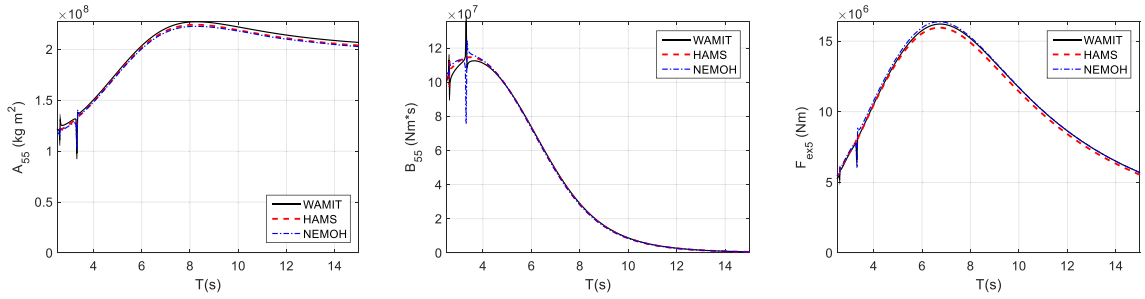

Fig. 15. Added mass (a), radiation damping coefficient (b) and wave excitation force (c) for pitch motion (TALOS device).

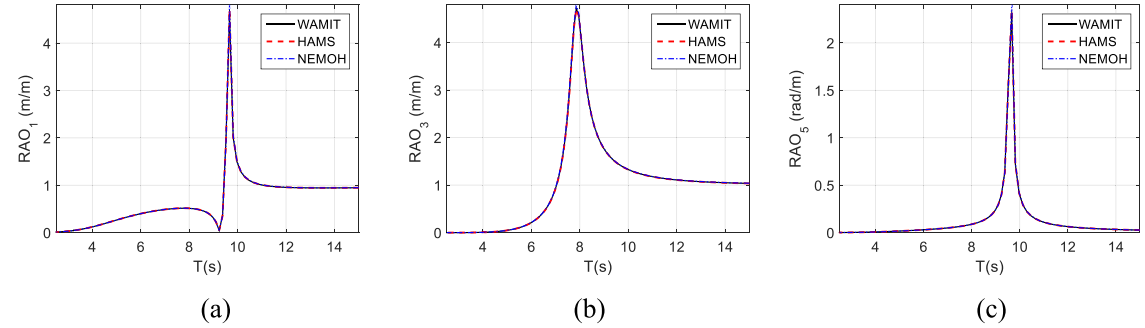

Fig. 16. RAOs for surge, heave and pitch motions of the truncated cylinder.

would predict the irregular parameters, such as the sharp variations in the added mass, the radiation damping coefficient.

If we compare the predictions for the surge motion with those of the simple truncated cylinder (compare Figs. 9–6), we can see the slight increases in hydrodynamic parameters have been introduced due to the heave plate, but the horizontal plate would not induce significant

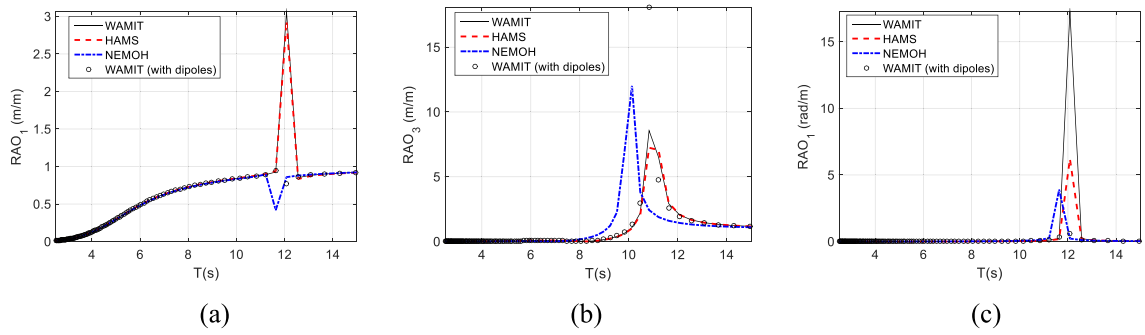

Fig. 17. RAOs for (a) surge, (b) heave and (c) pitch motions of truncated cylinder with a heave plate.

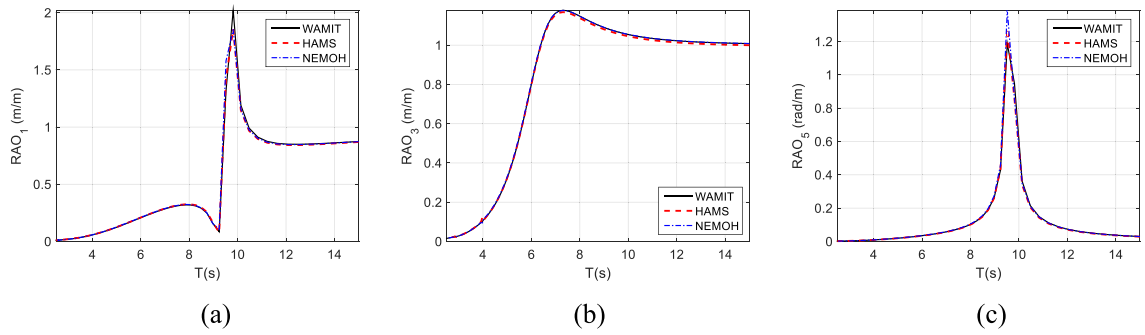

Fig. 18. RAOs for surge, heave and pitch motions of truncated cylinder with a heave plate.

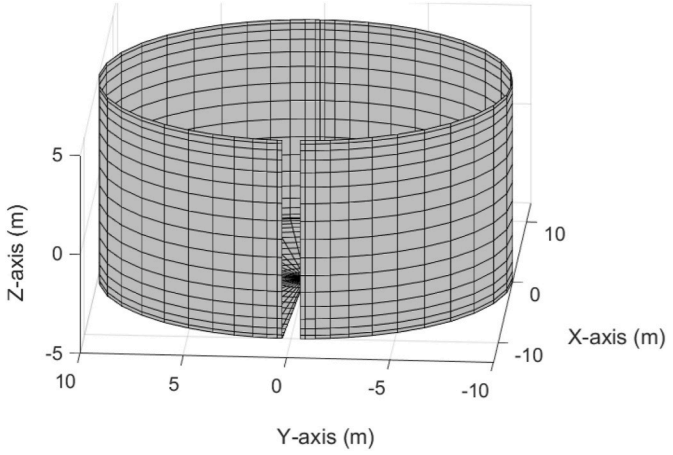

Fig. 19. Incomplete panels with a gap of 5°on the side and on the bottom of the cylinder. Total panels: 768 (with a symmetry about y-axis). Panel file can be downloaded from (Sheng, 2022).

changes in the surge motion, a horizontal motion.

Fig. 10 shows the hydrodynamic parameters for the heave motion of the truncated cylinder with a heave plate: the added mass, A_{33}, the radiation damping coefficient, B_{33}, and the wave excitation force, F_{ex3}. Here we can see NEMOH does not predict the hydrodynamic parameters for heave motion well. The large difference can be seen for the added mass, radiation damping coefficient and the wave excitation, and we can also see the negative radiation damping coefficients for some wave periods are predicted by NEMOH (see Fig. 7b), and such non-physical radiation damping coefficients can be also seen in the example of the cylinder with heave plates (see (Penalba et al., 2017)). In comparison, HAMS and WAMIT can handle the thin structure nicely. Both methods predict the hydrodynamic parameters very close to the predictions using dipoles. From this example, we can see HAMS may be a good choice for dealing with the thin structures.

Fig. 11 shows the hydrodynamic parameters for the pitch motion of the truncated cylinder with a heave plate: the added moment of inertia, A_{55}, the radiation damping coefficient, B_{55}, and the wave excitation moment, F_{ex5}. The trends are similar to those for the heave motion. Again, NEMOH fails to predict the relevant hydrodynamic parameters, probably due to the approximation method of the free surface Green function applied in NEMOH.

HAMS and WAMIT, with the panels for the thin plate, slightly overpredict the added moment of inertia, radiation damping coefficient and the wave excitation moment. HAMS also over-predicts these hydrodynamic parameters than WAMIT, although the difference is not large. It should be noted that using the real thin structure and using dipoles would cause the different centres of buoyancy, thus the different metacentric height (centres of gravity are set same for all cases), and thus the difference for the pitch motion.

If WAMIT (commercial) is not option in simulation, HAMS (open source) would be a choice for such a marine structure. The main reason may be in HAMS, very similar approach in approximating the free-surface Green function has been implemented (see the relevant references (Liu et al., 2015; Wu et al., 2018; Wu et al., 2017) and Table 1).

A discussion would be made here. The simulations in this research employ only the panel methods, which are based on potential flow theory. Indeed, the panel methods may give some good predictions on the added mass and radiation damping coefficients, while in reality the damping effects due to the viscous damping and due to the vortex induced damping are also important, as Subbulakshmi et al. in (Subbulakshmi and Sundaravadivelu, 2016) have shown the importance of the damping due to heave plates using both the experiment and CFD modelling. Hence a complete modelling shall include all these effects. This is especially true if the heave plates are used to suppress the motion of the cylinder or spar in waves (Tao and Cai, 2004). In the future study, using CFD modelling data to tune the additional damping coefficients for

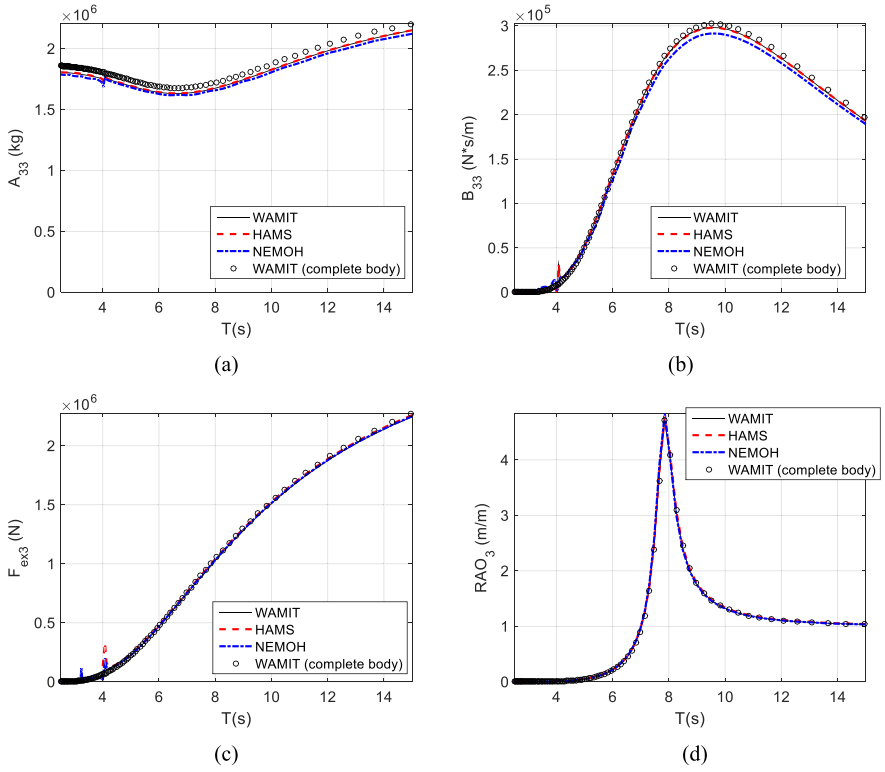

Fig. 20. Added mass, radiation damping, wave excitation and RAO of the incomplete truncated cylinder, with 'WAMIT (complete body)' meaning the WAMIT prediction for the complete truncated cylinder.

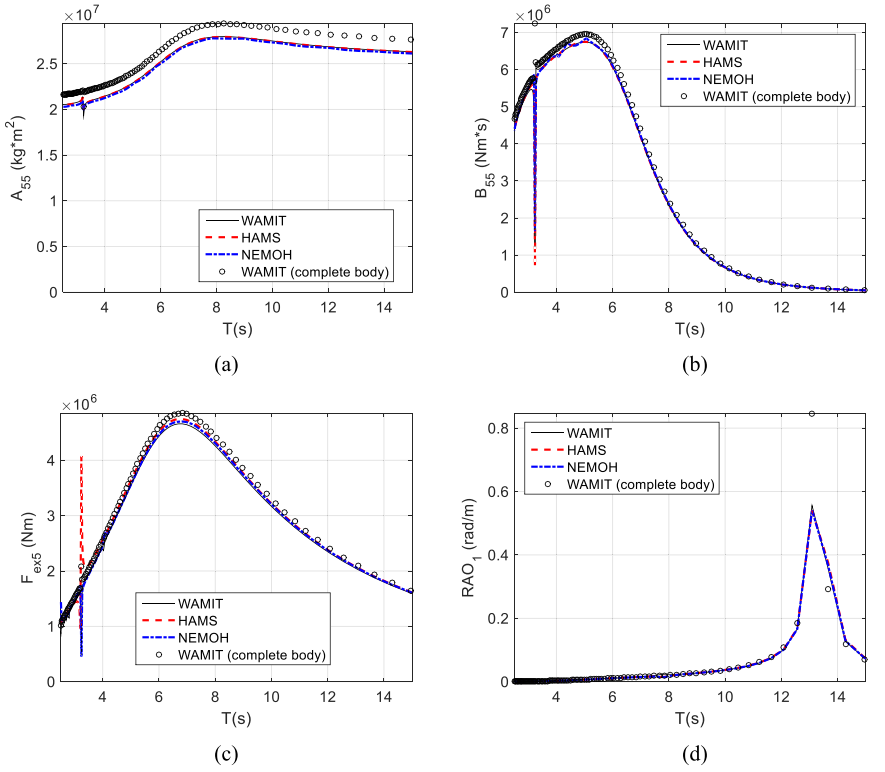

Fig. 21. Added moment of inertia, radiation damping, wave excitation moment and RAO of the incomplete truncated cylinder, with 'WAMIT (complete body)' meaning the WAMIT prediction for the complete truncated cylinder.

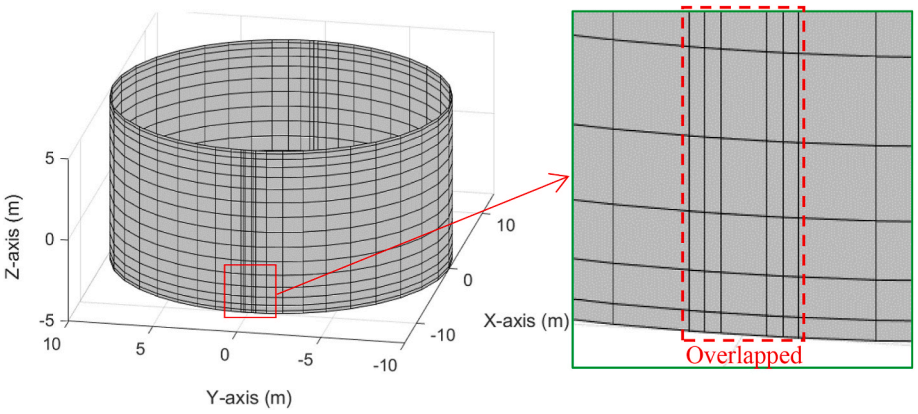

Fig. 22. Overlapped panels (overlapping of 5° on the side and on the bottom of the cylinder). Total panels: 768 (with a symmetry about y-axis). Panel file can be downloaded from (Sheng, 2022).

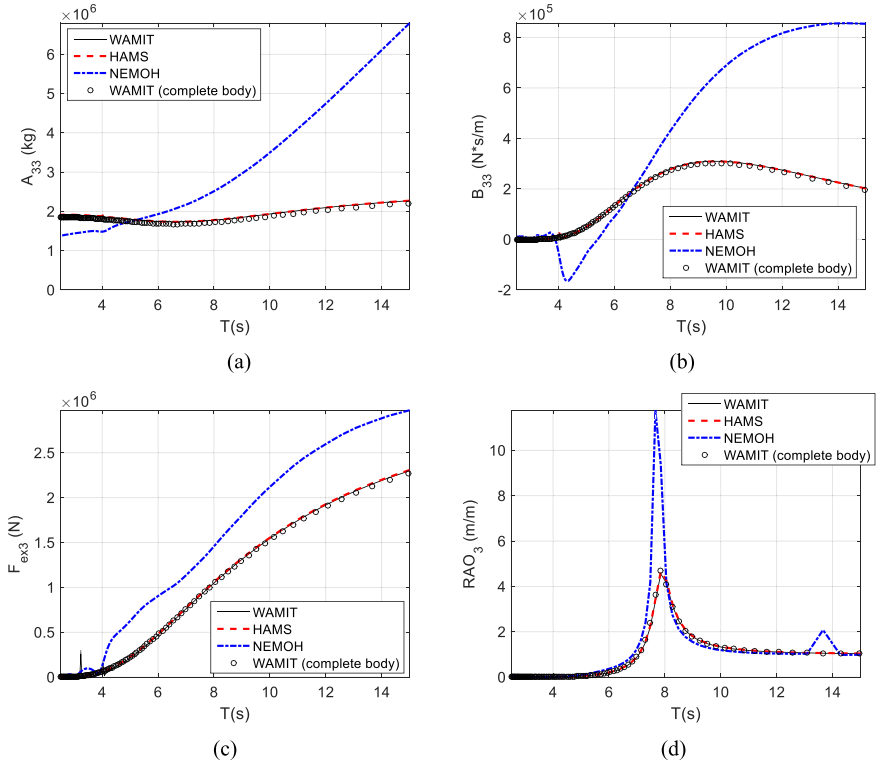

Fig. 23. Added mass, radiation damping, wave excitation and RAO of the overlapped truncated cylinder, with 'WAMIT (complete body)' meaning the WAMIT prediction for the complete truncated cylinder.

panel methods may allow an improved modelling for panel methods, while the computational time can be tiny when compared to the full CFD modelling.

3.2.3. TALOS point absorber

Fig. 12 shows the hydrodynamic parameters for the surge motion of the TALOS point absorber: the added mass, A_{11}, the radiation damping coefficient, B_{11}, and the wave excitation force, F_{ex1}. Fig. 13 shows the hydrodynamic parameters for the heave motion of the TALOS point absorber: the added mass, A_{33}, the radiation damping coefficient, B_{33}, and the wave excitation force, F_{ex3}. And Fig. 14 shows the hydrodynamic parameters for the pitch motion of the TALOS point absorber: the added moment of inertia, A_{55}, the radiation damping coefficient, B_{55}, and the wave excitation moment, F_{ex5}. It can be seen that the agreements of the predictions of WAMIT, NEMOH and HAMS are closer than those for the simpler marine structure, the truncated cylinder.

From Fig. 14, very small differences can be discerned in the hydrodynamic parameters in pitch motion when compare the predictions from NEMOH and HAMS to those from WAMIT. From Fig. 14a, we can see both NEMOH and HAMS slightly underpredict the added moment of inertia, while from Fig. 14c, HAMS slightly underpredicts the wave excitation moment, and NEMOH slightly overpredicts. For the radiation damping coefficients, they are almost identical, except for the short waves and at the irregular frequencies.

In the case of TALOS, the differences of the predictions from NEMOH and HAMS are very small, thus they can be all accepted in the applications in terms of modelling accuracy.

Table 2
Capacity comparison of WAMIT, NEMOH and HAMS.

Functionalities	WAMIT	NEMOH	HAMS
Free surface Green function	Mathematical approximation	Interpolation from the look-up table	Mathematical approximation
Symmetries	2 (about x- and y-axes)	1 symmetry	1 symmetry
Multi-bodies	Yes	Yes	No (in the current form)
Handling thin structure	Ok for thin structure (but a better option is with dipoles)	No	Ok for thin structure
Handling incomplete panels	Yes	yes	Yes
Handling overlapped panels	Yes	no	yes
Zero- and infinite-frequencies	Yes	no	Yes
Impulse functions	Yes (use FD2TD kit)	Yes	Can be easily done.
RAOs	Yes	No	Yes
Removal of irregular frequency	Yes	No	Yes
Generalized modes	Yes	No	No
High-order panels	Yes	No	No
Running time	Fast (100%)	Slow (~500%)	Fast (~77%)
Multi-core option	Yes (v70 and later)	no	yes
Interface	DOS commands	DOS commands (wrapped up in Matlab)	DOS commands

Table 3
Computational time (for 125 frequencies).

Code name	Core No.	Running time (s)
WAMIT	1 (multi-cores possible for new versions)	1395
NEMOH	1 (no option)	5620
HAMS	1 (multi-cores can be specified)	1076

3.3. Comparisons of motion responses

3.3.1. Truncated cylinder

The RAOs (response amplitude operators) for truncated cylinder are given in Fig. 15, and all RAOs predicted by the different software are very close, even at the peaks of the RAOs. In the surge RAO, the RAO peak happens at the wave period of $T = 9.7$s, which is same as the peak response in the pitch RAOs. In fact, the RAO peak seen in the surge response is a result of surge-pitch coupling. Also, we can see from the RAOs, the sharp variations in the added mass, damping coefficient and wave excitation at the irregular frequency have no influence in the motion responses.

3.3.2. Truncated cylinder with heave plate

For the truncated cylinder with a thin plate, similar to the hydrodynamic parameters as shown previously, NEMOH predicts RAOs quite differently, see Fig. 16. It can be seen that NEMOH could not predict the correct resonance periods, nor the magnitudes of the RAOs. For HAMS and WAMIT, both predict the resonance periods of all motions very close to the case of dipoles, although the magnitudes of the RAOs may not be well reproduced.

3.3.3. TALOS point absorber

Since we have seen the hydrodynamic parameters have been all well predicted by these three codes (see Fig. 12–14), the predictions of RAOs of the TALOS point absorber by all three codes are very close, see Fig. 17. All RAO predictions are almost identical, except the magnitudes at the resonance periods for pitch motions, and also the differences in surge RAOs, which may be caused by the differences in pitch motion, since surge and pitch are strongly coupled.

4. Hydrodynamic comparisons for incomplete and overlapped panels

In this section, the comparisons are made on 2 extreme cases: when the panels are generated in an incomplete manner and in an overlapped manner. In contrast to the computational fluid dynamics (CFD) modelling, where the establishment of the structure is generally very strict: neither the incomplete structure nor the overlapped structure may be allowed, although the staggered mesh may be used in the specific numerical algorithms. In here, we examine: 1) whether the numerical modelling of the panel methods can be carried out smoothly for those imperfect panels as those of the complete panels; 2) if so, whether the results would be very different from those complete panels. To make the comparison simpler, the truncated cylinder is studied.

4.1. Incomplete truncated cylinder

The incomplete panels can be seen on the truncated cylinder, see Fig. 18. We can see the gaps on the side and on the bottom of the cylinder: a gap of 5° out of 360 degrees of the full cylinder (about 1.39% surface is missing).

From Fig. 19 and Fig. 20, we can see for the incomplete panels, all codes would handle it nicely, and all give quite close results to the predictions of the complete cylinder with WAMIT.

From Fig. 19, for the heave motion, all codes slightly under-predict the added mass, and radiation damping coefficient, but the wave excitation and the response amplitude operator are very close. From Fig. 20, we can see slightly large differences for the pitch motion, especially in the added moment of inertia, otherwise they are very close each other.

From this example, we can see a slight incompletion of the panels may not cause large numerical modelling problems for the hydrodynamic studies of the structures, and the predicted results are quite good too. This may be good for modelling the complicated structures, since we may be allowed to leave some small gaps for the panels for the difficult small regions, instead of having to generate the complete panels. Otherwise, we may have to buy the specific software for generating the complete panels for the junctions of the complicated structure components. After all, we are supposed to use the open source software to solve our modelling problems.

4.2. Overlapped truncated cylinder

The overlapped panels can be seen on the truncated cylinder, see Fig. 21. We intentionally generate the overlapped panels on the side and on the bottom of the cylinder (overlapped for 5° out of 360 degrees of the cylinder, see the overlapped panels in Fig. 21).

For the overlapped panels, both WAMIT and HAMS can handle the modelling effectively. From Fig. 22 and Fig. 23, we can see WAMIT and HAMS predict all the hydrodynamic parameters very close to those of the complete panels, while NEMOH predicts them very differently, including the negative radiation damping coefficients (the non-physical values). The reason for this may be in the calculation of free surface Green function. In NEMOH, it is calculated using the look-up table and the interpolation to get Green function. However, for the overlapped panels, the source panel and the target panel could be overlapped. That means the distance between them could be very close to zero or very small, thus it could cause the difficulties in the numerical modelling. In

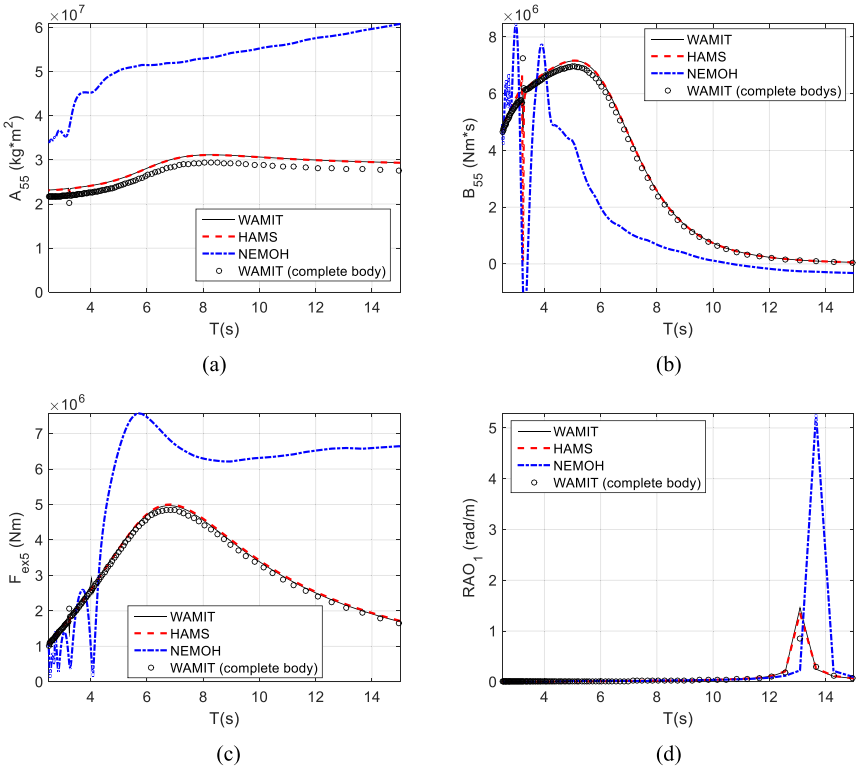

Fig. 24. Added moment of inertia, radiation damping, wave excitation moment and RAO of the overlapped truncated cylinder, with 'WAMIT (complete body)' meaning the WAMIT prediction for the complete truncated cylinder.

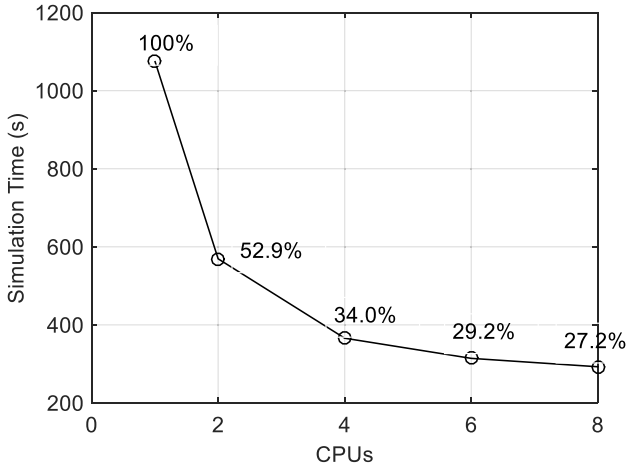

Fig. 25. Simulation time in seconds vs CPUs (HAMS).

contrast, in WAMIT and HAMS, the free surface Green function is mathematically approximated, even when the source panel and the field panel are very close. This is very similar to the case of the cylinder with a thin plate.

5. Software performance comparisons

In the section, the summaries would be given for the comparisons of the software performance. This includes the software capacity comparison, mostly for the functionalities of the respective software; and the speed comparison, for which the numerical modelling of each code is clocked simply from the start to the end of the numerical modelling.

5.1. Capacity comparison

As a commercial code, WAMIT is generally regarded as the most used panel code, since it implements many very useful functionalities (than most other commercial codes), and it is generally regarded as one of the best of the kind, while as the open source software, both NEMOH and HAMS may be good enough for some simple structures, but they also have many limits: some limits are different, while some others are same. However, but for many practical marine structures, both NEMOH and HAMS can provide the useful hydrodynamic parameters.

In Table 2, a summary is given for the main capacities of WAMIT, NEMOH and HAMS in wave-structure interactions.

5.2. Speed comparison

The speed comparison is simply carried out for a reference, mainly for the relative speed in the numerical modelling of the panel codes on a desktop, on which all the numerical simulations have been conducted. The desktop specifications are as follows: CPU: Intel Core (TM) - i7-2600 @3.40GHz (4 cores, 8 processors); installed physical memory (RAM) of 24.0 GB; a GPU: AMD Radeon HD 7700 Series.

The comparisons are for the TALOS point absorber: the total panels are 1632 with one symmetry (same panels for all simulations), and the wave frequencies are 125. In the speed comparison, all the numerical simulations are carried out using single core of CPU.

It can be seen from Table 3, HAMS is actually faster than WAMIT, using about 77% time as WAMIT, while NEMOH would take 4 times long as the WAMIT.

The running time using different cores in HAMS can be seen in Fig. 24. Taking the running time of single core as 100%, then using 2 cores, the running time would be reduced to 52.7%; 34% for 4 cores and 27.2% for 8 cores. For the above specified computer with 8 virtual cores, using cores more than 4 does not seem very beneficial (see Fig. 25).

In this numerical modelling, if we use 4 cores in HAMS, then it would

take only about 1/15th time of NEMOH (only one core can be used). In this regard, using HAMS could save a lot of time if we have many simulations to be carried out. In fact, in this comparison work, a lot of time has been on waiting for the NEMOH results.

6. Conclusions

The aims of the research work are twofold: first, by the comparisons of the open source software on three different structures, this research wishes to show the capacities of the open source codes, as well as their limitations. As a result, it could provide researchers some guidance for choosing an open source code so to meet the requirements for their numerical modelling. The second is for choosing a suitable open source code for the TALOS hydrodynamic modelling, and for the optimisation of the TALOS wave energy converter. TALOS multi-axis wave energy converter is a single body structure, but we wish to have a fast, reliable and accurate open source panel method, and additionally in the future, we may also add some enhancements for the wave energy converter.

From the studies for examining the capacities of the different open source codes, in brief, the conclusions could be summarised as follows:

- HAMS has implemented the approximation method of the free-surface Green function as those in WAMIT, thus the accuracy and speed of the simulations are better than NEMOH, in which only the look-up table and the interpolation method are employed, thus the accuracy may be reduced, in addition to the slow speed in the simulation.
- For the simple marine structures, that is, those marine structures without thin structures or overlapped panels, all BEM methods (WAMIT, NEMOH and HAMS) could provide very good and close predictions of the hydrodynamic parameters.
- For the body with thin structure (heave plate), HAMS and WAMIT can both handle it nicely (when compare to the result of WAMIT using dipoles), while NEMOH could not predict the hydrodynamic parameters correctly. The main reason is probably in NEMOH, the look-up table and the interpolation method are not accurate enough when the source and field point are very close.
- For the incomplete panels, all three codes could handle the problems very nicely. This may be good for the researchers if they have to generate the panels on the complicated marine structures, it may simplify the panel generation by leaving some small gaps, even the incomplete panels would be acceptable.
- For some other marine structures, panels may be generated in an overlapped manner, for instance, at the joints of the structures. For such overlapped panels, both WAMIT and HAMS can handle it without big issues, while NEMOH could not deal with it correctly. Again, this may be caused by the different methods for calculating the free surface Green function.
- As the open source software, HAMS is better than NEMOH, in both accuracy and speed, but it also has a huge limit in its current form: it can only model single structures. If multi-bodies are the target, NEMOH is the only available open source code.

It should be noted that both HAMS and NEMOH are still in development, and it is hoped that more functionalities would be implemented in HAMS and NEMOH to make them better in future. For instance, the NEMOH developer once outlined the plans to improve NEMOH (Babarit and Delhommeau, 2015), but we must say the improvements have been very slow. From the website, there are no updates since 2016 (Nemoh, 2021).

For your reference, the relevant mesh files have been available to public (Sheng, 2022). The available mesh files include: the simple truncated cylinder; the cylinder with heave plate; the incomplete mesh of the cylinder; and the overlapped mesh for the cylinder.

CRediT authorship contribution statement

W. Sheng: Conceptualizsation, Methodology, Software, calculation, Formal analysis, and . **E. Tapoglou:** Writing – review & editing. **X. Ma:** Writing – review & editing. **C.J. Taylor:** Writing – review & editing. **R. M. Dorrell:** Writing – review & editing. **D.R. Parsons:** Writing – review & editing. **G. Aggidis:** Conceptualization, Project administration, Resources, Supervision, Writing – review & editing.

Declaration of competing interest

The authors declare that they have no known competing financial interests or personal relationships that could have appeared to influence the work reported in this paper.

Acknowledgements

This work was supported by the EPSRC, Grant number EP/V040561/1, UK for the project Novel High Performance Wave Energy Converters with advanced control, reliability and survivability systems through machine-learning forecasting (NHP-WEC).

References

Aggidis, G.A., Taylor, C., 2017. J., Overview of wave energy converter devices and the development of a new multi-axis laboratory prototype. IFAC-PapersOnLine 50–1, 15651–15656. https://doi.org/10.1016/j.ifacol.2017.08.2391.

Babarit, A., Delhommeau, G., 2015. Theoretical and Numerical Aspects of the Open Source BEM Solver NEMOH. presentation at EWTEC 2015. cited on: 01/09/2021. https://www.researchgate.net/publication/282288245_Theoretical_and_numerical_aspects_of_the_open_source_BEM_solver_NEMOH.

Brown, A., Thomson, J., Rusch, C., 2017. Hydrodynamic coefficients of heave plates, with application to wave energy conversion. IEEE J. Ocean. Eng. https://doi.org/10.1109/JOE.2017.2762258.

Evans, D.V., Jeffrey, D.C., Taylor, J.R.M., 1979. Submerged cylinder wave energy device: theory and experiment. Appl. Ocean Res. 1 (1), 3–12. https://doi.org/10.1016/0141-1187(79)90003-8.

Falcao, A., Henriques, J.C.C., Candido, J.J., 2012. Dynamic and optimization of the OWC spar buoy wave energy converter. Renew. Energy 48, 369–381. https://doi.org/10.1016/j.renene.2012.05.009.

Greenhow, M., Ahn, S.I., 1988. Added mass and damping of horizontal circular cylinder sections. Ocean Eng. 15 (5), 495–504. https://doi.org/10.1016/0029-8018(88)90012-1.

Kim, D., Chen, L., Blaszkowski, Z., 1999. Linear frequency domain hydroelastic analysis for McDermott's mobile offshore base using WAMIT. In: Proceedings of the 3rd International Workshopon Very Large Floating Structures (VLFS '99). Hawaii, USA, Honolulu.

Liu, Y., 2020. HAMS: an Open-Source Computer Program for the Analysis of Wave Diffraction and Radiation of Three-Dimensional Floating or Submerged Structures cited on: 19/10/2021. https://github.com/YingyiLiu/HAMS.

Liu, Y., 2021. Introduction of the open-source boundary element method solver HAMS to the ocean renewable energy community. In: Proceedings of the 14th European Wave and Tidal Energy Conference, 5-9 Sep. 2021. Plymouth, UK.

Liu, Y., Iwashita, H., Hu, C., 2015. A calculation method for finite depth free-surface green function. Int. J. Naval Archit. Ocean Eng. 7, 375–389. https://doi.org/10.1515/ijnaoe-2015-0026.

Nemoh. NEMOH-Presentation. cited on: 01/10/2021. https://lheea.ec-nantes.fr/valorisation/logiciels-et-brevets/nemoh-presentation.

Newman, J.N., 1977. Marine Hydrodynamics. The MIT Press, Cambridge, Massachusetts, USA.

Newman, J.N., 1985. Algorithms for free-surface Green function. J. Eng. Math. 19, 57–67. https://doi.org/10.1007/BF00055041.

Newman, J.N., 1992. The approximation of free-surface Green functions. In: Martin, P.A., Wickham, G.R. (Eds.), In Wave Asymptotics; Retirement Meeting for Professor Fritz Ursell, University of Manchester. Cambridge University Press, *Cambridge, UK*, pp. *107–135*, 1992.

Parisella, G., Gourlay, T.P., 2016. Comparison of Open-Source Code Nemoh with Wamit for Cargo Ship Motions in Shallow Water. Curtin University, Australia cited on: 03/07/2017. http://cmst.curtin.edu.au/wp-content/uploads/sites/4/2015/06/Parisella-Gourlay-2016-Comparison-of-open-source-code-Nemoh-with-Wamit-for-cargo-ship-motions-in-shallow-water.pdf.

Penalba, M., Kelly, T., Ringwood, J.V., 2017. Using NEMOH for modelling wave energy converters: a comparative study with WAMIT. In: Proceedings of 12th European Wave and Tidal Energy Conference, 28th Aug-1st Sep, 2017. Cork, Ireland.

Robertson, A., et al., 2016. OC5 project phase ib: validation of hydrodynamic loading on a Fixed,Flexible cylinder for offshore wind applications. Energy Proc. 94, 82–101. https://doi.org/10.1016/j.egypro.2016.09.201.

ANSYS. Ansys AQWA. cited on: 01/10/2021. https://www.ansys.com/training-center/course-catalog/structures/introduction-to-ansys-aqwa.

Sheng, W., 2022. Mesh files for WAMIT, NEMOH and HAMS. cited on: 12/02/2022. https://zenodo.org/record/6053524.
Subbulakshmi, A., Sundaravadivelu, R., 2016. Heave damping of spar platform for offshore wind turbine with heave plate. Ocean Eng. 121, 24–36. https://doi.org/10.1016/j.oceaneng.2016.05.009.
WAMIT. User manual (v73). cited on: 01/11/2021. https://www.wamit.com/manualupdate/v73_manual.pdf.
Tao, L., Cai, S., 2004. Heave motion suppression of a Spar with a heave plate. Ocean Eng. 31 (5–6), 669–692. https://doi.org/10.1016/j.oceaneng.2003.05.005.
Tao, L., Thiagarajan, K.P., Cheng, L., 2000. On the parametric dependence of springing damping of TLP and Spar columns. Appl. Ocean Res. 22 (5), 281–294. https://doi.org/10.1016/S0141-1187(00)00017-1.
WAMIT. WAMIT ltd. cited on: 07/10/2021. https://www.wamit.com/.
Wang, Y., et al., 2008. Theoretical research on hydrodynamics of a geometric spar in frequency- and time-domains. J. Hydrodyn. Ser. B 20 (1), 30–38. https://doi.org/10.1016/S1001-6058(08)60024-4.
Wu, H., et al., 2017. A global approximation to the Green function for diffraction radiation of water waves. Eur. J. Mech. B Fluid 65, 54–64. https://doi.org/10.1016/j.euromechflu.2017.02.008.
Wu, H., Liang, H., Noblesse, F., 2018. Wave component in the Green function for diffraction radiation of regular water waves. Appl. Ocean Res. 81, 72–75. https://doi.org/10.1016/j.apor.2018.10.006.
Zhang, D., et al., 2015. Wave tank experiments on the power capture of a multi-axis wave energy converter. J. Mar. Sci. Technol. 20, 520–529. https://doi.org/10.1007/s00773-015-0306-5.